PCDA™ SLAM-BASED TECHNOLOGY FOR POINT CLOUD AND TRAJECTORY OPTIMIZATION FOR AIRBORNE, LAND, AND INDOOR APPLICATIONS IN GNSS-DENIED ENVIRONMENTS.

M.M.R. Mostafa[1 *], M. Sever[2], V. Huynh[1], N. Jaeger[3], A. Jarvis[1], J. Hutton[1], S. Kurz[4]

[1] Trimble Applanix, 85 Leek Cr., Richmond Hill, Ontario, Canada L4B 3B3 (mmostafa, vhuynh, ajarvis, jhutton)@applanix.com
[2] Trimble Germany GmbH, Arnulfstrasse 126, Germany - msever@applanix.com
[3] Trimble Germany GmbH, An der Wuhlheide 232 A, 12459 Berlin, Germany – njaeger@applanix.com
[4] Trimble Germany GmbH, Obere Stegwiesen 26, 88400 Biberach, Germany - sven_kurz@trimble.com

KEY WORDS: Trimble Applanix PCDA™, SLAM, GNSS, LiDAR point cloud data, trajectory data, check point RMS

ABSTRACT:

This paper presents the results of assessing the performance of Trimble Applanix PCDA™ SLAM-based technology to simultaneously optimize any mobile mapping system trajectory and LiDAR point cloud data in a GNSS-denied environment. The simultaneous use of inertially-aided GNSS data along with LiDAR point clouds to optimally correct shifts and/or drifts in the trajectory in GNSS-denied environments is addressed in detail in this paper. A number of Trimble MX50 Mobile Mapping System data sets were acquired in Germany particularly to assess the performance of PCDA™. The land mobile mapping data sets were acquired in deep urban canyons which were purposely acquired that way to reach the most challenging land mobile mapping data sets in a GNSS-denied environment. The PCDA™ technology assessment results are presented in detail. In summary, the results show how LiDAR data can successfully be used to correct the trajectory shifts and drifts due to GNSS outages by simultaneously optimizing both point cloud and trajectory data.

1. INTRODUCTION

Airborne, land, and indoor geospatial data acquisition has been used for decades to produce accurate 3D mapping products (c.f., El-Sheimy, 1996 for land mobile mapping systems, Ip et al, 2007 for land mobile mapping systems, Mostafa and Schwarz, 1999, 2000, 2001 for crewed airborne systems, Mostafa, 2017 for uncrewed systems). Elhashash, et al, 2022 and Aoki, et al, 2012 listed a variety of applications for mobile mapping systems that all use the same payload and system architecture. are being used for a variety of applications.

Today, it is typical, when using autonomous platforms such as drones, and robotic land vehicles to leverage multiple sensors including GNSS, inertial measuring units, LiDAR, Cameras, etc. for 3D reality capture. The data from the sensor payloads are georeferenced using a high-rate position and orientation solution computed by combining measurements from GNSS, IMUs, odometers, magnetometers, cameras, and LiDAR (c.f., Hutton, et al, 2016).

The typical method for this multi-sensor integration is using an Aided-Inertial Kalman Filter based architecture in which the data is post-processed, which offers the advantages of processing the data both in the forward and reverse directions. Recent expansions of the GNSS constellations (including BeiDou III) has resulted in over 100 satellites with multiple frequencies in full operation that can now be used for accurate positioning in what were previously marginal conditions.

In addition, the introduction of low-cost, high-performance, miniaturized LiDAR scanners now provides a cost-effective method of measuring relative position and orientation that can be used to correct drifts in the trajectory in GNSS-denied environments. Trimble's Applanix POSPacTM 9 software using Trimble© ProPointTM GNSS, Trimble CenterPoint© RTX, Applanix IN-Fusion+™, and Applanix PCDA™ technology is an advanced Aided-Inertial post-processing software package that has been optimized for mobile mapping and surveying applications in all environments.

Today, it is normal for systems to include multiple cameras and LiDARs integrated with Inertially-aided GNSS (c.f., Ravi et al, 2016). Trimble Applanix PCDA™ technology is based on a Simultaneous Localization and Mapping (SLAM) algorithm. PCDA™ works with any type of LiDAR sensor and a variety of GNSS and inertial measuring units.

It voxelizes the LiDAR data into a number of levels (c.f., Bosse and Zlot, 2009; Cummins, and Newman, 2008) from which it does planar detection and correspondence that is then used in conjunction with the trajectory in order to calibrate different system parameters such as boresight, lever arms between different sensors (c.f., Mirzaei et al, 2012), while it optimizes the trajectory and point cloud in an optimized Least Squares environment as shown in Figure 1.

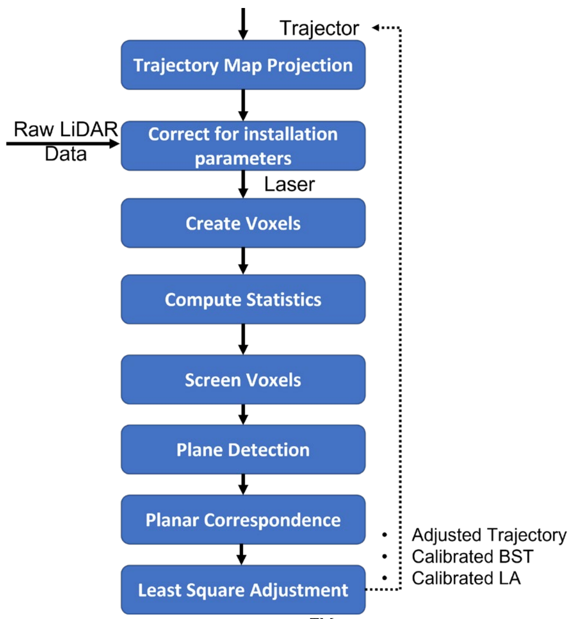

Figure 1: PCDA™ Workflow

2. DATA DESCRIPTION

This section is dedicated to describing the data used for the analysis presented in this paper. The system used in data acquisition along with its technical specifications are listed in the following subsections together with a description of the data acquisition mechanism.

2.1 Mobile Mapping System Configuration

Trimble MX50 mobile mapping system (shown in Figure 2) is used to acquire the data used in the analysis presented in this paper. The system specifications are listed in Table 1 for the laser sensors and Table 2 for the GNSS-Inertial georeferencing sensors.

Figure 2: Trimble MX50 Mobile Mapping System

MX50 LASER SCANNER	
Number of laser scanners	2
Laser class	1, eye-safe
EFFECTIVE MEASUREMENT RATE[2]	320 kHz and 960 kHz
Scan speed (Dual Head system)	240 scans/sec
Maximum range, target reflectivity > 80 %[3]	80 m
Minimum range	0.6 m
Maximum number of targets per pulse	1
Range accuracy[4]/Precision[5]	2 mm/2.5 mm @ 30 m
Field of view[6]	Full 360°

Table 1: Trimble MX50 Technical Specifications

EMBEDDED TRIMBLE GNSS-INERTIAL SYSTEM		
IMU Options	AP60	AP20
ACCURACY—NO GNSS OUTAGES (POST PROCESSED)[7]		
X, Y Position (m)	0.020	0.020
Z Position (m)	0.050	0.050
Velocity (m/s)	0.005	0.005
Roll and Pitch (deg)	0.005	0.015
Heading (deg)[8]	0.015	0.025
ACCURACY—60 SECOND GNSS OUTAGE (POST PROCESSED)[7]		
X, Y Position (m)	0.100	0.320
Z Position (m)	0.070	0.130
Roll and Pitch (deg)	0.005	0.020
Heading (deg)[8]	0.015	0.030

Table 2: Trimble MX50 Embedded GNSS-Inertial System Specifications

2.2 Data Acquisition Configuration

The analysis presented in this paper is based on a data set acquired in Biberach, Germany (shown in Figure 3). The MX50 was driven for an approximately 350 m twice in the same direction in order to end up with an overlap for the LiDAR data shown in the green color-coded trajectory shown in Figure 3. The data was acquired three different times.

The three individual data sets are referred to here as Data 338, Data 342, and Data 344, respectively.

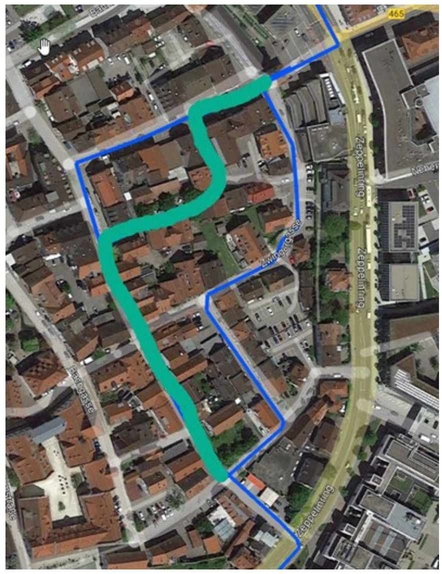

Figure 3: Trajectory of the MX50 data set acquired in Biberach, Germany

The data set was intentionally acquired in an area with many medium-rise buildings which resulted in substandard GNSS intervisibility between the TMX50 GNSS receiver's antenna and different satellite antennas.

This resulted in the following (as shown in Figure 4):

1. The number of GNSS satellites was significantly different between the two passes due to the time difference between the two drives over the same road segment,
2. The number of satellites in less than four satellites in many epochs of the data in one pass over the same road segment. On the other hand, the number of satellites is a little higher (from 2 to 6 satellites) in the second pass over the same road segment.

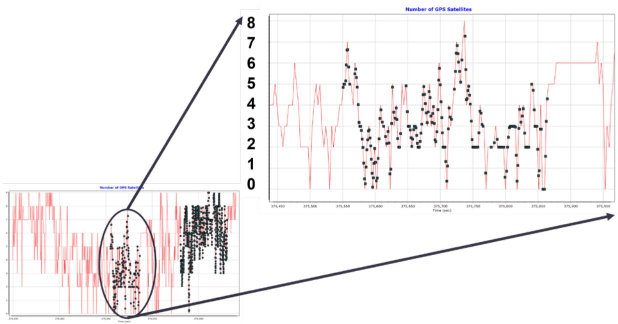

Figure 4: Number of GNSS Satellites acquired in the Biberach MX50 Data.

Note that LiDAR point cloud accuracy is influenced by a number of parameters in addition to the trajectory accuracy, including the technical specifications of the Inertial Measuring Unit (IMU) used in the system and the accuracy and validity of the installation parameters (including boresight angles and lever arms).

3. DATA PROCESSING RESULTS AND ANALYSIS

This section is dedicated to describe two data processing workflows and their associated results and analysis.

3.1 Data Processing Without PCDA™

In this standard data processing workflow, POSPac™ has been used to process the raw GNSS/Inertial Data in order to produce a Smoothed Best Estimate of the Trajectory (SBET) for the two different passes over the same road segment of approximately 350 m. Subsequently, the SBET data has been used to Georeference the LiDAR data for the two different passes over the same road segment.

This resulted in two different LiDAR point clouds covering the same road segment. A number of cross sections were taken in the LiDAR point clouds in order to analyse the influence of the different GNSS satellite sky configuration during the two different passes.

Figure 5 shows a vertical cross section taken in a wall in the LiDAR point cloud in the first pass (red) as well as another vertical cross section taken in the same wall in the second point cloud. Please note that the two passes are covering the same road segment. It is noticeable that there is a spatial horizontal distance (error) between the two cross sections of the same wall of up to 12 cm.

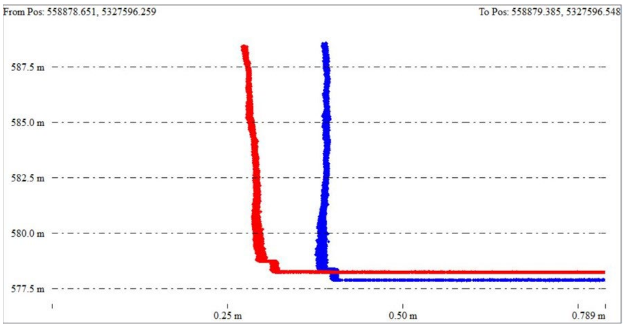

Figure 5: LiDAR Point Cloud Vertical Cross Sections showing Pass #1 (red) and Pass #2 (blue)

Figure 6 shows a cross section taken in the pavement in the LiDAR point cloud in the first pass (red) as well as another cross section taken across the same pavement in the point cloud of the second pass (blue). Please note that the two passes are covering the same road segment. It is noticeable that there is a spatial vertical distance (error) between the two cross sections of the same pavement of up to 30 cm.

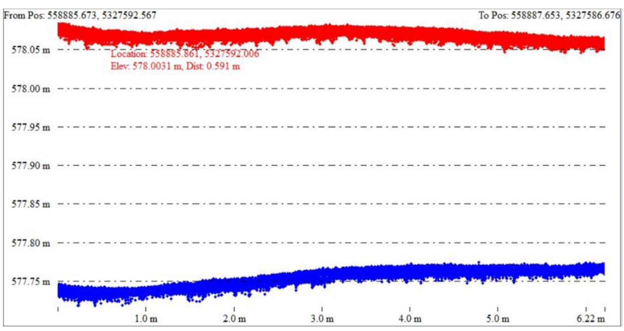

Figure 6: LiDAR Point Cloud Pavement Cross Sections showing Pass #1 (red) and Pass #2 (blue)

3.2 Data Processing Optimization Using PCDA™

In this standard data processing workflow, POSPac™ has been used to process the raw GNSS/Inertial Data in order to produce an SBET for the two different passes over the same road segment of approximately 350 m. Subsequently, the SBET data has been used to Georeference the LiDAR data for the two different passes over the same road segment, but this time PCDA™ has been used to optimize both the LiDAR point cloud and the SBET.

This resulted in optimizing the two different LiDAR point clouds covering the same road segment. Figure 7 shows a vertical cross section taken in a wall in the LiDAR point cloud in the optimized first pass (green) as well as another vertical cross section taken in the same wall in the optimized second point cloud.

It is noticeable that both wall cross sections happened to coincide due to the minimal spatial distance (error) between them which is down to a horizontal error of up to 1 cm.

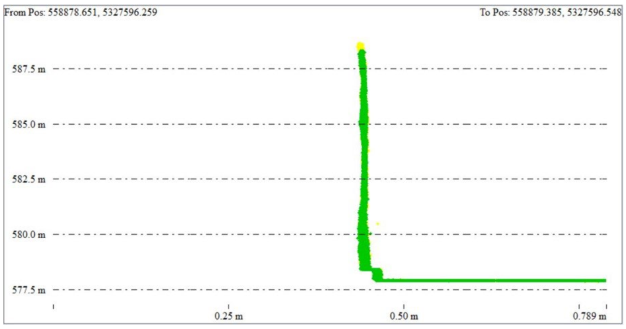

Figure 7: LiDAR Point Cloud Vertical Cross Sections showing Pass #1 (green) and Pass #2 (yellow) using PCDA™

It is obvious that using PCDA™ resulted in a much smaller error in the order of 1 cm shown in Figure 7. Using the same data set and same processing workflow without PCDA™ resulted in an error of up to 12 cm as shown in Figure 5.

It is clear that using the standard LiDAR point cloud processing without PCDA™ does not use the overlapping LiDAR point clouds covering the same road segment and, thus, when driving a mobile mapping system in a GNSS-denied environment for more that a certain threshold would influence the individual point cloud accuracy.

When using PCDA™, on the other hand, the nature of overlapping LiDAR point clouds allowed for optimizing the trajectory to improve the GNSS-denied environment influence on the LiDAR point cloud accuracy.

However, an outstanding question arises. Does PCDA™ average the overlapping point clouds acquired from different passes. In order to address this question, the before and after PCDA™ results were plotted together in the same plot as shown in Figure 8. Upon examining the cross sections taken across the same wall in the two different passes of MX50 vehicle over the same road segment, the following can be concluded:

- PCDA™ does not average the errors in the point clouds due to the rather poor GNSS data due to the exposure to the GNSS-denied environment.
- The optimized LiDAR point cloud is not an average of the non-optimized point cloud as shown in Figure 8

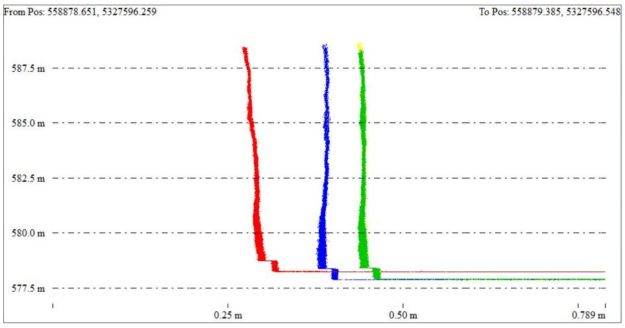

Figure 8: LiDAR Point Cloud Vertical Cross Sections showing Pass #1 (red) and Pass #2 (blue) *before* PCDA™ and Pass #1 (green) and Pass #2 (yellow) *after* PCDA™

Figure 9 shows a pavement cross section of the LiDAR point cloud in the optimized first pass (green) as well as another pavement cross section taken in the same road pavement in the optimized second point cloud.

It is noticeable that both pavement cross sections happened to coincide due to the minimal spatial distance (error) between them which is down to a vertical error of up to 2 cm. It is obvious that using PCDA™ resulted in a much smaller error in the order of 2 cm shown in Figure 9. Using the same data set and same processing workflow without PCDA™ resulted in an error of up to 30 cm as shown in Figure 6.

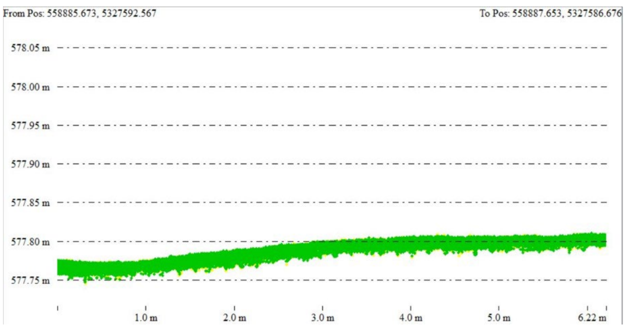

Figure 9: LiDAR Point Cloud Pavement Cross Sections showing Pass #1 (green) and Pass #2 (yellow) using PCDA™

3.3 Check Point Analysis Before and After Using PCDA™

A large number of accurate Ground Control Points (GCP) has been established for various testing purposes of the Trimble MX50 Mobile Mapping System in Biberach, Germany. In this Section, the three data sets analysed in this paper were used to assess the final accuracy of the check points before and after using PCDA™.

There Trimble MX50 data sets acquired in Biberach, Germany, were used to assess the check point residuals before and after using PCDA™ to optimize the LiDAR point cloud and the SBET data, namely:

- Data 338,
- Data 342, and
- Data 344.

Figure 10 shows the check point residuals RMS for the three abovementioned data sets without using PCDA™.

The horizontal errors range from 2 cm to 15 cm while the vertical errors range from 3 cm to 28 cm.

Figure 11 shows the check point residuals RMS for the three abovementioned data sets after using PCDA™. Both horizontal and vertical RMS are at the level of 2-3 cm on average.

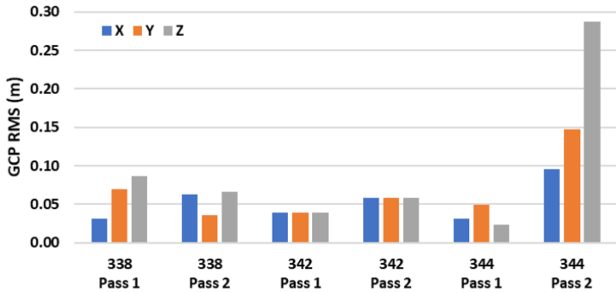

Figure 10: Check Point Residuals Before Using PCDA™

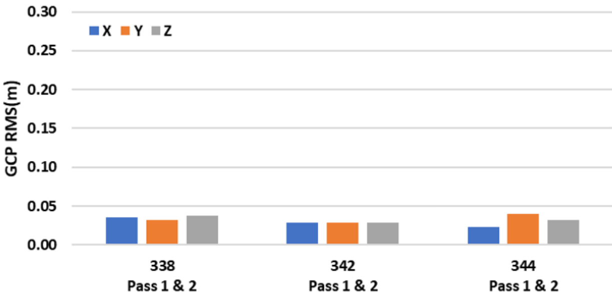

Figure 11: Check Point Residuals Before Using PCDA™

Note that before using PCDA™, the check point residuals for each data set are different from Pass 1 to Pass 2. After using PCDA™, however, the difference between pass 1 and Pass 2 is less than 1 cm and therefore both passes of each data set are presented in one bar for each coordinate component.

3.4 Visual Analysis of Point Cloud Data Sets Before and After Using PCDA™

Point cloud visual analysis took place for the three data sets analysed here. Figure 12 shows a plan (top-down) view of the LiDAR point cloud showing road markings before using PCDA™.

It seems that horizontal errors tend to appear in different parts of the point cloud based on the GNSS data quality/availability that is reflected in the form of deteriorated processed SBET accuracy that adversely influence the LiDAR point cloud final accuracy.

Figure 13 shows the same plan (top-down) view of the LiDAR point cloud showing the same road markings after using PCDA™. Multiple of these visual inspections were done across the entire road segment of about 350 m in the three data sets analysed in this paper.

Even though visual analysis cannot constitute a quantitative analytical method, but it is still worth mentioning that across the three data sets, every single issue captured in the visual analysis similar to that shown in Figure 12, has been resolved after using PCDA™.

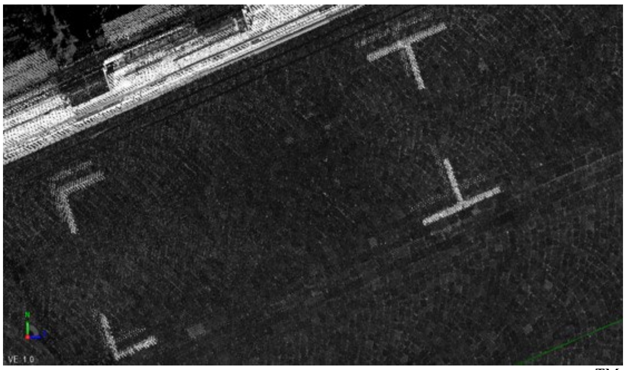

Figure 12: LiDAR Point Cloud Sample Before Using PCDA™

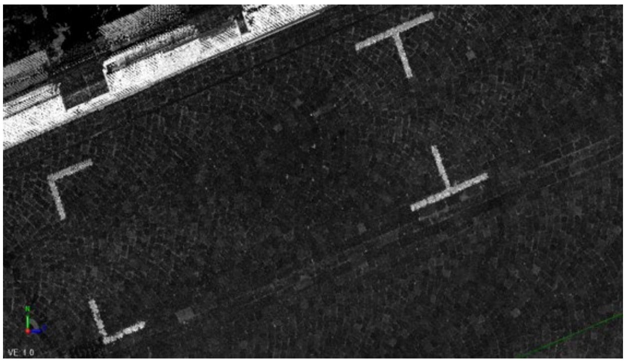

Figure 13: LiDAR Point Cloud Sample After Point Cloud and SBET Optimization Using PCDA™

SUMMARY AND CONCLUSIONS

In this paper, Trimble Applanix PCDA™ technology has been briefly presented. Additionally, three data sets acquired in Biberach, Germany were used to analyse the performance of PCDA™. The three data sets were acquired using Trimble MX50 Mobile Mapping System.

The three data sets were acquired in the same road segment of approximately 350 m by driving the mobile mapping system vehicle on the same road segment twice in the same direction for each data set in order to create overlapped LiDAR point clouds.

In conclusion, using PCDA™ to assess the three data sets acquired particularly for this analysis resulted in consistently simultaneously optimizing the LiDAR point cloud data and the trajectory data. The following can be concluded:

1. PCDA™ improved the LiDAR Point Cloud internal consistency between two different mobile mapping passes over the same road segment from 12 cm to 1 cm in horizontal and from 30 cm to 2 cm in elevation.
2. PCDA™ improved the check point RMS from (2-15 cm) horizontal error to (2-3 cm).
3. PCDA™ improved the check point RMS from (3-28 cm) vertical error to (2-3 cm).

REFERENCES

Aoki, K., Yamamoto, K., and Shimamura, H., 2012. Evaluation model for pavement surface distress on 3D point clouds from mobile mapping system. *Int. Arch. Photogramm. Remote Sens. Spat. Inf. Sci.* 2012, XXXIX-B3, 87–90.

Bosse, M. and Zlot, R., 2009. Keypoint design and evaluation for place recognition in 2D lidar maps, *Robotics and Autonomous Systems*, Volume 57, Issue 12, 2009, Pages 1211-1224, ISSN 0921-8890, https://doi.org/10.1016/j.robot.2009.07.009.

Cummins, M. and Newman, P., 2008. FAB-MAP: Probabilistic localization and Mapping in the Space of Appearance. *International Journal of Robotics Research*, vol. 27, no. 6, pp. 647–665, June 2008.

Jaakkola, A., Hyyppä, J., Kukko, A., Yu, X., Kaartinen, H., Lehtomäki, M., and Lin, Y., 2010. A low-cost multi-sensoral mobile mapping system and its feasibility for tree measurements. *ISPRS J. Photogramm. Remote Sens*. 2010, 65, 514–522.

Elhashash, M.; Albanwan, H.; and Qin, R., 2022. A Review of Mobile Mapping Systems: From Sensors to Applications. *Sensors* 2022, 22, 4262. https://doi.org/10.3390/s22114262

El-Sheimy N., 1996. A Mobile Multi-Sensor System For GIS Applications In Urban Centers. *Int. Arch. Photogramm. Remote Sens. Spatial Inf. Sci.*, XXXI-B2, pp. 95-100.

Hutton, J., N. Gopaul, X. Zhang, J. Wang, V. Menon, D. Rieck, A. Kipka, F. Pastor, 2016. Centimeter-Level, Robust GNSS-Aided Inertial Post-Processing For Mobile Mapping without Local Reference Stations. *Int. Arch. Photogramm. Remote Sens. Spatial Inf. Sci.*, XLI-B3, 2016. https://doi.org/10.5194/isprs-archives-XLI-B3-819-2016

Ip, A., N. El-Sheimy, and M.M.R. Mostafa, 2007. Performance Analysis of Integrated Sensor Orientation. *PE&RS*, 73 (1): 89 – 97.

Mirzaei F.M., Kottas D.G., and Roumeliotis, S.I., 2012. 3D LIDAR–camera intrinsic and extrinsic calibration: Identifiability and analytical least-squares-based initialization. *The International Journal of Robotics Research*. 31(4):452-467. DOI:10.1177/0278364911435689

Mostafa, M.M.R., 2017. Accuracy Assessment of Professional Grade Unmanned Systems for High Precision Airborne Mapping. *Int. Arch. Photogramm. Remote Sens. Spatial Inf. Sci.*, XLII-2/W6, 257–261, https://doi.org/10.5194/isprs-archives-XLII-2-W6-257-2017

Mostafa, M.M.R. and K.P. Schwarz, 2001. Digital image georeferencing from a multiple camera system by GPS/INS. *ISPRS Journal of Photogrammetry & Remote Sensing* 56 (2001): 1-12.

This contribution has been peer-reviewed.
https://doi.org/10.5194/isprs-archives-XLVIII-1-W1-2023-333-2023

Mostafa, M.M.R. and K.P. Schwarz, 2000. A Multi-Sensor System for Airborne Image Capture and Georeferencing. *PE&RS*, 66 (12): 1417-1424.

Mostafa, M.M.R. and K-P Schwarz, 1999. A GPS/INS/Imaging System for Kinematic Mapping in Fully Digital Mode, Proceedings, The IUGG 99 Congress, Birmingham, UK, July 18-30, 1999.

Ravi, R., Lin, Y.–J., Elbahnasawy, M., Shamseldin, T., and Habib, A., 2018. Simultaneous System Calibration of a Multi–LiDAR Multicamera Mobile Mapping Platform. *IEEE Journal of Selected Topics in Applied Earth Observations and Remote Sensing*, 11(5), 1694–1714. https://doi.org/10.1109/JSTARS.2018.2812796

Verma, S., Berrio, J. S., Worrall, S., & Nebot, E. (2019). Automatic Extrinsic Calibration Between a Camera and a 3D Lidar Using 3D Point and Plane Correspondences. IEEE Intelligent Transportation Systems Conference, ITSC 2019. https://doi.org/10.1109/ITSC.2019.8917108

Zhou, T., Cheng, Y-T, Shin, S-Y, Shin, S-H, Hodaei, M, Liu, J and Habib, A. (2023) Unified Multi–Sensor Advanced Triangulation (UMSAT) for System 1 Calibration and Trajectory Enhancement of Imaging and Ranging Sensors 2 Onboard Mobile Mapping Systems, Proceedings, FIG Working Week, Orlando, FL, USA, 28 May - 1 June 2023